JOURNAL OF MAGNETIC RESONANCE, Series B 101, 194–197 (1993)

Measurement of $^3J_{HN\alpha}$ Vicinal Coupling Constants in Proteins

M. GÖRLACH,* M. WITTEKIND,† B. T. FARMER II,‡ LEWIS E. KAY,§ AND LUCIANO MUELLER†

*Howard Hughes Medical Institute, University of Pennsylvania, Philadelphia, Pennsylvania 19104-6148; † Bristol-Myers Squibb, Pharmaceutical Research Institute, P.O. Box 4000, Princeton, New Jersey 08543-4000; ‡Department of Research and Development, NMR Instruments, Varian Associates, 3120 Hansen Way, Palo Alto, California 94304; and §Departments of Medical Genetics, Biochemistry, and Chemistry, University of Toronto, Toronto, Canada

Received August 14, 1992; revised October 30, 1992

Vicinal J couplings represent an additional source of structural information in proteins by providing estimates of torsion angle constraints. Recently, ^1H, ^{13}C, ^{15}N triple-resonance[1] (*1–5*) and ^1H, ^{13}C (*6–10*) double-resonance experiments have been proposed that permit the measurement of J couplings in labeled proteins by exhibiting E.COSY-like (*11*) fine structures in cross peaks with multiplet components separated by the large $^1J(H-^{13}C)$ couplings and the $^3J(H-H)$ couplings in their respective frequency domains. All of these experiments provide accurate coupling constants in peptides and small proteins. However, in larger proteins small errors may occur in the observed J couplings due to relaxation effects. In this report we will show that distorted J-coupling values are generally expected in these techniques (*1–10*). In addition, a modified pulse sequence is presented which minimizes distortions caused by relaxation effects, thereby yielding more accurate values of $^3J_{NH\alpha}$.

It was not obvious at the outset of our study whether proton cross-relaxation pathways between the t_1 evolution period and the detection period would give rise to systematic errors in the observed $^3J_{NH\alpha}$ splittings. For this reason, J couplings were remeasured with slightly different pulse schemes as depicted in Fig. 1.

In the following paragraphs the relevant coherence pathways of the sequences depicted in Fig. 1 are written in terms of product operators. First, amide proton magnetization is transferred to the amide nitrogen by an INEPT (*12*) transfer (Figs. 1A and 1B) or by a DEPT transfer (Figs. 1C and 1D). Subsequently ^{15}N coherence evolves during the first evolution period t_2,

$$\sigma(t_2) = N_y I_z \sin(\pi\, {}^1J_{NH}\delta)\cos(\omega_N t_2), \quad [1]$$

where $N = {}^{15}N$ and $I = {}^1H_N$.

Next, $^{15}N-^{13}C$ coupling terms develop during Δ,

$$\sigma(t_2, \Delta) = N_x I_z C_z \sin(\pi\, {}^1J_{NH}\delta)\sin(\pi\, {}^1J_{NC}\Delta)\cos(\omega_N t_2), \quad [2]$$

where $C = {}^{13}C_\alpha$, neglecting modulation due to the $^1J_{NH}$ coupling, which is refocused at time point d.

At the beginning of the second evolution period t_1 (time point b in Figs. 1A and 1B), the N_xC_z term is converted into $^{15}N-^{13}C$ multiple-quantum coherence, which then evolves under the influence of the carbon chemical-shift Hamiltonian and the $^1J_{C\alpha H\alpha}$ coupling. The relevant term of the nitrogen–carbon multiple-quantum coherence can be written, in terms of the population of molecules with the $^1H_\alpha$ spin up, as

$$\sigma(t_2, \Delta, t_1) = N_x I_z C_y[E + 2A_z] \times F(\delta, \Delta)\cos(\omega_N t_2)\cos[(\omega_C + \pi\, {}^1J_{CH})t_1] \quad [3a]$$

and, in terms of the population with the $^1H_\alpha$ spin down, as

$$\sigma(t_2, \Delta, t_1) = N_x I_z C_y[E - 2A_z] \times F(\delta, \Delta)\cos(\omega_N t_2)\cos[(\omega_C - \pi\, {}^1J_{CH})t_1], \quad [3b]$$

where $A = H_\alpha$, $E = 2(A^\alpha + A^\beta)$, $A_z = (A^\alpha - A^\beta)$, and $F(\delta, \Delta) = \sin(\pi\, {}^1J_{NH}\delta)\sin(\pi\, {}^1J_{NC}\Delta)$.

Subsequently, the coherence described in Eq. [3] is transferred back to the amide proton in close analogy to the HNCA experiment (*13*). After the application of the carbon read pulse, the ^{15}N coherence evolves under the influence of the one-bond couplings to the C_α carbon and the amide proton. At time step d in Figs. 1A and 1B, the density operator can be written, for the population of molecules with the $^1H_\alpha$ spin up, as (retaining only the relevant terms)

$$\sigma(t_2, \Delta, t_1, \Delta) = N_z I_z[E + 2A_z]\cos(\omega_N t_2) \times \cos[(\omega_C + \pi\, {}^1J_{CH})t_1]F(\delta, \Delta)\sin(\pi\, {}^1J_{NC}\Delta) \quad [4a]$$

and, for the population of molecules with the $^1H_\alpha$ spin down, as

$$\sigma(t_2, \Delta, t_1, \Delta) = N_z I_z[E + 2A_z]\cos(\omega_N t_2) \times \cos[(\omega_C - \pi\, {}^1J_{CH})t_1]F(\delta, \Delta)\sin(\pi\, {}^1J_{NC}\Delta). \quad [4b]$$

[1] Preliminary data were presented at the 30th Eastern Analytical Symposium, Somerset, New Jersey, Nov. 18, 1991.

1064-1866/93 $5.00

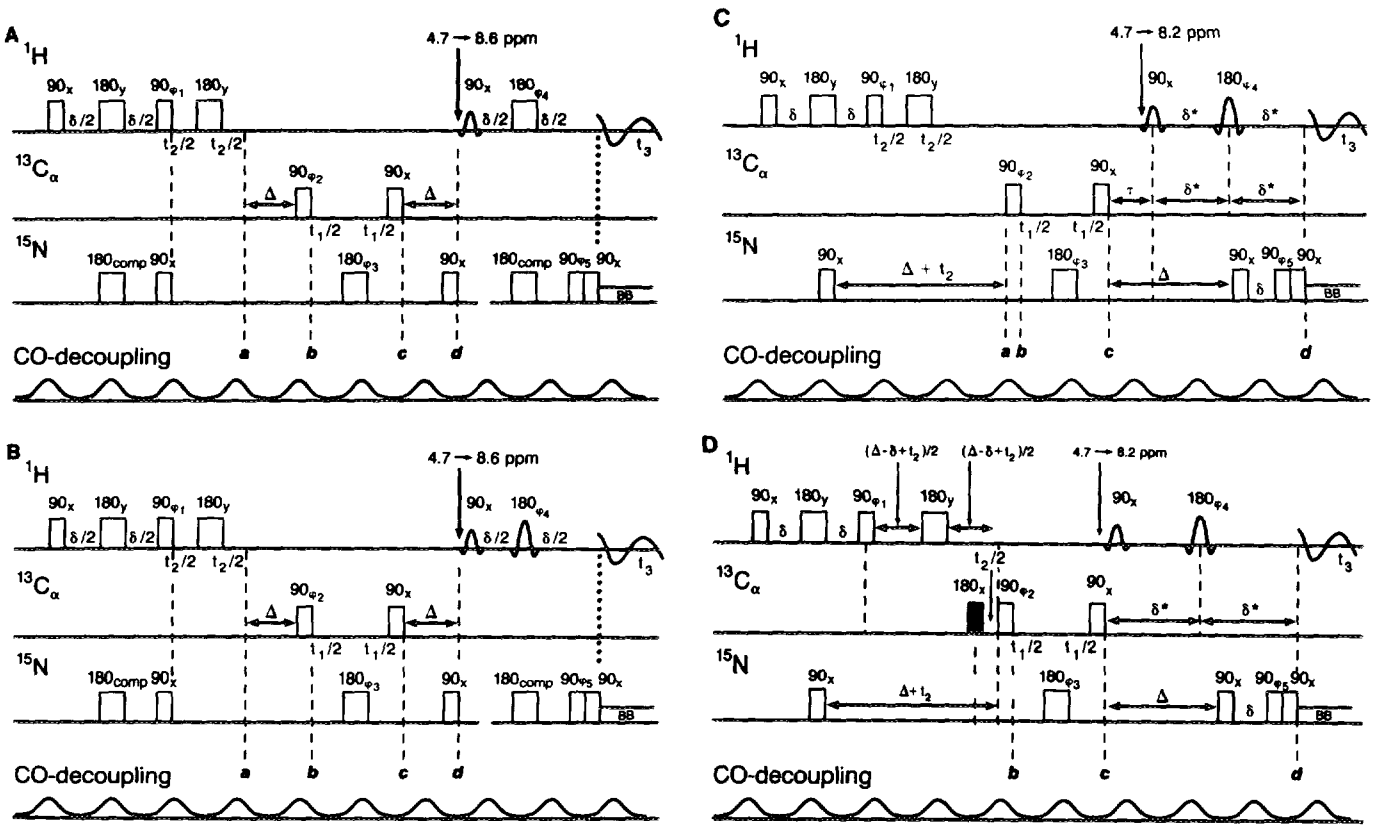

FIG. 1. Pulse sequences used to measure $^3J_{HN\alpha}$ coupling constants: δ = 4.5 ms, Δ = 21.6, $\tau = 1/(2\,^1J_{NH})$ = 5.4 ms, $\delta^*(D) = [\Delta + \delta]/2$ = 13.05 ms, $\delta^*(C) = [\delta^*(D) - \tau/2]$ = 10.35 ms. The length of all Hermite pulses was approximately 1.3 ms with the amplitude of the 180° pulse being twice the amplitude of the 90° pulse, whose peak amplitude was set to approximately 0.7 kHz. Phase cycling was as follows: $\phi_1 = (y, -y)$, $\phi_2 = 2(x), 2(-x)$, $\phi_3 = 4(x), 4(y), 4(-x), 4(-y)$, $\phi_4 = 8(x), 8(-x), 8(y), 8(-y)$, $\phi_5 = 8(x), 8(-x)$; receiver phase = $(A, -A, A, -A)$, where $A = (x, -x, -x, x, -x, x, x, -x)$. The observe frequency was set on the resonance of the solvent peak during both presaturation and the t_1 and t_2 evolution periods and was coherently switched to the center of the amide region prior to the application of the selective Hermite pulses.

In the subsequent reverse INEPT transfer of nitrogen coherence to amide proton magnetization, perturbation of the $^1H_\alpha$ proton is minimized by the use of a pair of frequency-selective Hermite pulses (Fig. 1B) (*14*) in lieu of a TANGO pulse (*15*), which requires extra delays.

The detected amide coherence for the population of molecules with the $^1H_\alpha$ spin up then can be written as

$$\sigma(t_2, t_1, t_3) = I_-[E + 2A_z]F^2(\delta, \Delta)\cos(\omega_N t_2) \times \cos[(\omega_C + \pi\,^1J_{CH})t_1] \times \exp\{-i(\omega_{NH} + {}^3J_{NH\alpha})^* t_3 + \Phi\} \quad [5a]$$

and for populations of molecules with the $^1H_\alpha$ spin down as

$$\sigma(t_2, t_1, t_3) = I_-[E - 2A_z]F^2(\delta, \Delta)\cos(\omega_N t_2) \times \cos[(\omega_C - \pi\,^1J_{CH})t_1] \times \exp\{-i(\omega_{NH} - {}^3J_{NH\alpha})^* t_3 - \Phi\}, \quad [5b]$$

where $\Phi = \pi\,^3J_{NH\alpha}\delta$ for the sequence depicted Fig. 1A and $\Phi = 0$ for all the other sequences in Fig. 1.

These results show that accurate $^3J_{NH\alpha}$ can be measured in small peptides where dipolar relaxation between the t_1 evolution period and the detection period can be neglected. Any flips of $^1H_\alpha$ between t_1 and t_3 due to dipolar relaxation attenuate the A_z term. The disappearance of this term corresponds to an equalization of magnetization within the $^1J_{CH}$ doublets, suggesting that proton dipolar relaxation during the back-transfer of coherence to the amide proton tends to convert E.COSY-type cross peaks, as depicted in Fig. 2, into clover-leaf-type DQF COSY patterns. In high-molecular-weight proteins, where the proton linewidths exceed the observed $^3J_{NH\alpha}$ splittings, this mixing of the two branches of the J doublets results in shifting the peak maxima toward the center of the cross peaks along the horizontal ^1H_N frequency axis F_3 (see Fig. 2). In a 21 kDa protein, the term N_xA_z is expected to relax almost twice the rate of N_x, causing a detectable error in the observed J value (*16*).

In the sequences depicted in Figs. 1C and 1D, the nitrogen–carbon multiple-quantum coherence described in Eq. [3] is converted into proton–nitrogen multiple-quantum coherence immediately after the end of t_1 (time point c in Fig. 1D) or after the subsequent period $\tau = 1/(2\,^1J_{NH})$ in Fig. 1C.

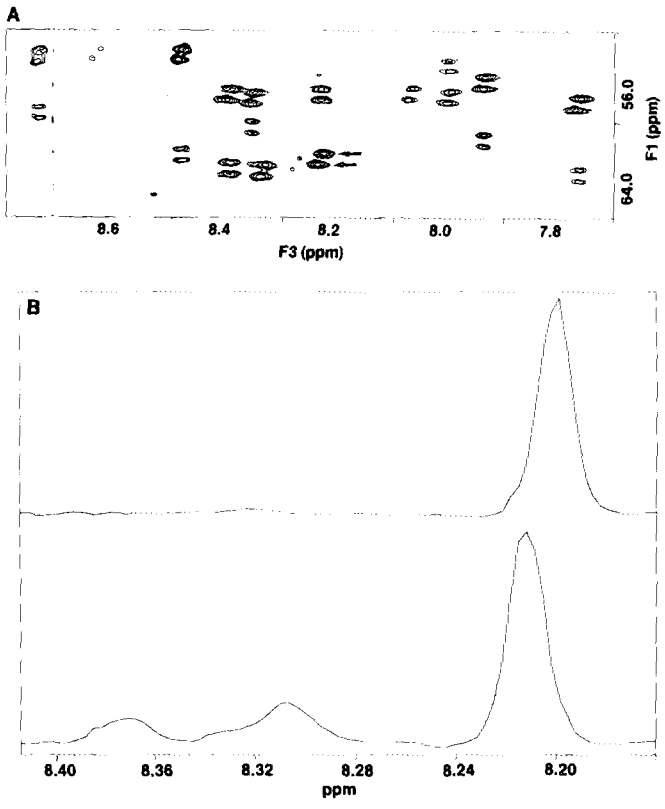

FIG. 2. Three-dimensional HNCA J spectrum of [^{15}N, ^{13}C]-enriched hnRNP C1 RNA-binding fragment, 2 mM at pH 5.5 in sodium acetate buffer: temperature = 20°C, ni(t_1) = 32, ni(t_2) = 28, np(t_3) = 1216, sw1 = 3000 Hz, sw2 = 2000 Hz, and sw3 = 4000 Hz. The lengths of the t_1 and t_2 interferograms were doubled using complex linear prediction. Skewed, i.e., exponentially attenuated, 40°-shifted sine-bell apodization was applied in t_3, 45°-shifted sine bell was applied in t_1, and 90°-shifted sine bell was applied in t_2 prior to Fourier transformation. (A) F_1(^{13}C), F_3(^{1}H) slice at F_2 = 125.7 ppm; (B) cross sections along F_3 at the location of the arrows in A.

The relevant coherence for the population of molecules with $^1H_\alpha$ up at time point c in the sequence in Fig. 1D can be written as

$$\sigma(t_2, t_1) = C_z N_x I_z[E - 2A_z] \times F(\delta, \Delta)\cos(\omega_N t_2)\cos[(\omega_C - \pi\,{}^1J_{CH})t_1], \quad [6b]$$

and for the population of molecules with $^1H_\alpha$ down as

$$\sigma(t_2, t_1) = C_z N_x I_z[E - 2A_z] \times F(\delta, \Delta)\cos(\omega_N t_2)\cos[(\omega_C - \pi\,{}^1J_{CH})t_1], \quad [6b]$$

where I = ^1H_N. The subsequent selective proton 90$^\circ_x$ pulse converts the N_xI_z terms into heteronuclear zero- and double-quantum transitions.

At the beginning of the acquisition time (time point d in Fig. 1D), the relevant term for the population of molecules with $^1H_\alpha$ up can be written as

$$\sigma(t_2, t_1, \Delta, \delta) = I_x[E + 2A_z] \times F^2(\delta, \Delta)\cos(\omega_N t_2)\cos[(\omega_C + \pi\,{}^1J_{CH})t_1] \quad [7a]$$

and for the population of molecules with $^1H_\alpha$ down as

$$\sigma(t_2, t_1, \Delta, \delta) = I_x[E - 2A_z] \times F^2(\delta, \Delta)\cos(\omega_N t_2)\cos[(\omega_C - \pi\,{}^1J_{CH})t_1]. \quad [7b]$$

During the detection period the density operator described in Eq. [6a] evolves into

$$\sigma(t_2, t_1, t_3) = I_-[E + 2A_z]F^2(\delta, \Delta)\cos(\omega_N t_2) \times \cos[(\omega_C + \pi\,{}^1J_{CH})t_1] \times \exp\{-i(\omega_{NH} + {}^3J_{NH\alpha})t_3\} \quad [8a]$$

and Eq. [6b] evolves into

$$\sigma(t_2, t_1, t_3) = I_-[E - 2A_z]F^2(\delta, \Delta)\cos(\omega_N t_2) \times \cos[(\omega_C - \pi\,{}^1J_{CH})t_1] \times \exp\{-i(\omega_{NH} - {}^3J_{NH\alpha})t_3\}. \quad [8b]$$

In a 15 kDa protein, the terms $N_{x,y}I_{x,y}$ and $N_{x,y}I_{x,y}A_z$ as depicted in Eq. [6] are expected to relax at more comparable rates corresponding to T_2 values of approximately 30 and 24 ms, respectively, resulting in a smaller bias in the observed J splitting. Nevertheless, a certain error in the observed J couplings remains, since the terms $I_{x,y}A_z$ always relax at a faster rate than $I_{x,y}$ in large molecules. For this reason we expect all methods that extract J couplings from E.COSY-type cross-peak patterns to provide biased J values in high-molecular-weight compounds.

The proposed experiments were first tested on a sample of [^{15}N, ^{13}C]-enriched Ac-Gly-Ala-OMet using an array of proton carrier frequencies in order to test the selectivity of the Hermite pulses. The use of a hard echo pulse (Fig. 1A) in the reverse INEPT transfer prior to the acquisition period in lieu of a selective Hermite pulse yielded the same observed J splittings, justifying the use of a selective Hermite echo pulse. All sequences in Fig. 1 provided the same coupling constants for the model peptide.

The sequences in Figs. 1B and 1C were used to measure the $^3J_{HN\alpha}$ coupling constants in a [^{15}N, ^{13}C]-enriched sample of the RNA-binding domain of hnRNP protein C1, for which a 3D structure has been recently obtained using heteronuclear 3D and 4D spectroscopy (*17*). A representative [^{1}H, ^{13}C] slice of the HNCA J spectrum using the sequence in Fig. 1B is presented in Fig. 2A. Cross sections along F_3 through the peaks highlighted by the arrows are depicted in Fig. 2B. The separation along F_3 (^{1}H axis) of the peaks depicted in Fig. 2B corresponds to $^3J_{NH\alpha}$. Clean, absorption-mode lineshapes are obtained with the sequences in Figs. 1B–1D, since the

TABLE 1
Values of Coupling Constants Measured in hnRNP C1 (*12*) Using the Sequences in Figs. 1B and 1C

Res.	Sequence in Fig. 1B	Sequence in Fig. 1C
Arg17	5.3	4.4
Val18	7.2	7.2
Phe19	4.2	4.3
Ile20	7.5	7.4
Asn22	6.5	8.4
Leu23	5.6	6.1
Val44	8.2	9.1
Cys46	4.4	5.5
Val48	7.1	7.3
His49	8.0	8.9
Ala53	6.1	6.6
Phe54	5.6	6.7
Val55	8.2	7.7
Gln56	8.1	8.3
Tyr57	7.3	7.9
Val58	7.3	8.2
Asn59	6.4	6.6
Leu80	2.8	3.0
Asp81	7.5	7.5
Ile82	7.6	8.6
Asn83	3.4	3.1
Leu84	3.0	3.0
Ala85	3.0	2.2

Hermite echo pulse (see Fig. 1) refocuses both chemical-shift and proton spin–spin interactions. The accuracy of the J values can be improved by inverse Fourier transformation of cross sections along the F_3 axis followed by zero-filling, resolution enhancement, and Fourier transformation.

Table 1 lists observed J values in the β-sheet domains of hnRNP C using the sequences in Figs. 1B and 1C. As expected, the sequence in Fig. 1C yields on average slightly larger J values. The observed coupling constants are in qualitative agreement with the previously elucidated secondary structural features in this protein—small J values of <5 Hz are observed in the α helices and predominantly large J values > 7 Hz in the β sheets (*17*). (see Table 1).

Resolution in both F_1 and F_2 was enhanced by extending the t_1 and t_2 interferograms using complex linear prediction (*18*). Carbonyl decoupling during the entire experiment was achieved by homonuclear selective decoupling (*19*).

We have shown that accurate $^3J_{NH\alpha}$ coupling constants can be measured in proteins using the HNCA J pulse scheme in peptides and small proteins. In proteins of high molecular weight, however, the observed splittings are biased toward smaller values due to differential relaxation of the coherences that form the observed cross peaks in the 3D spectrum. Modified pulse schemes are proposed that provide more accurate values at the expense of lower sensitivity.

REFERENCES

1. (*a*) G. T. Montelione and G. Wagner, *J. Am. Chem. Soc.* **111,** 5474 (1989); (*b*) G. T. Montelione, S. D. Emerson, and B. A. Lyons, *Biopolymers* **32,** 327 (1992).
2. L. E. Kay and A. Bax, *J. Magn. Reson.* **86,** 110 (1990).
3. G. T. Montelione and G. Wagner, *J. Magn. Reson.* **87,** 183 (1990).
4. O. W. Sørensen, *J. Magn. Reson.* **90,** 433 (1990).
5. G. Wagner, P. Schmieder, and V. Thanabal, *J. Magn. Reson.* **93,** 436 (1991).
6. G. Gemmecker and S. Fesik, *J. Magn. Reson.* **95,** 208 (1991).
7. S. D. Emerson and G. T. Montelione, *J. Am. Chem. Soc.* **114,** 354 (1992).
8. G. T. Montelione, S. D. Emerson, and B. A. Lyons, *Biopolymers* **32,** 327 (1992).
9. C. Griesinger and U. Eggenberger, *J. Magn. Reson.* **97,** 426 (1992).
10. S. D. Emerson and G. T. Montelione, *J. Magn. Reson.* **99,** 413 (1992).
11. (*a*) C. Griesinger, O. W. Sørensen, and R. R. Ernst, *J. Am. Chem. Soc.* **107,** 6394 (1985); (*b*) C. Griesinger, O. W. Sørensen, and R. R. Ernst, *J. Chem. Phys.* **85,** 6387 (1986).
12. G. A. Morris and R. Freeman, *J. Am. Chem. Soc.* **101,** 760 (1979).
13. L. E. Kay, M. Ikura, R. Tschudin, and A. Bax, *J. Magn. Reson.* **89,** 496 (1990).
14. W. S. Warren, *J. Chem. Phys.* **81,** 5437 (1984).
15. S. Wimperis, and R. Freeman, *J. Mag. Reson.* **58,** 348 (1984).
16. S. Campbell-Burk, P. Domaille, and L. Mueller, *J. Magn. Reson.* **93,** 171 (1991).
17. M. Wittekind, M. Görlach, M. Friedrichs, G. Dreyfuss, and L. Mueller, *Biochemistry* in press (1992).
18. E. T. Olejniczak, and H. L. Eaton, *J. Magn. Reson.* **87,** 628 (1990).
19. (*a*) M. A. McCoy, and L. Mueller, *J. Am. Chem. Soc.* **114,** 2108 (1992); (*b*) M. A. McCoy, and L. Mueller, *J. Magn. Reson.* in press (1992).